

# Journal Pre-proof

Low temperature synthesis of bio-fuel additives via valorisation of glycerol with benzaldehyde as well as furfural over a novel sustainable catalyst, 12-tungstosilicic acid anchored to ordered cubic nano-porous MCM-48

Anjali Patel (Conceptualization) (Writing - review and editing) (Supervision), Dhruvi Pithadia (Methodology) (Software)<ce:contributor-role>Writing-original draft) (Writing - review and editing)



PII: S0926-860X(20)30322-7

DOI: <https://doi.org/10.1016/j.apcata.2020.117729>

Reference: APCATA 117729

To appear in: *Applied Catalysis A, General*

Received Date: 19 April 2020

Revised Date: 30 June 2020

Accepted Date: 2 July 2020

Please cite this article as: Patel A, Pithadia D, Low temperature synthesis of bio-fuel additives via valorisation of glycerol with benzaldehyde as well as furfural over a novel sustainable catalyst, 12-tungstosilicic acid anchored to ordered cubic nano-porous MCM-48, *Applied Catalysis A, General* (2020), doi: <https://doi.org/10.1016/j.apcata.2020.117729>

This is a PDF file of an article that has undergone enhancements after acceptance, such as the addition of a cover page and metadata, and formatting for readability, but it is not yet the definitive version of record. This version will undergo additional copyediting, typesetting and review before it is published in its final form, but we are providing this version to give early visibility of the article. Please note that, during the production process, errors may be discovered which could affect the content, and all legal disclaimers that apply to the journal pertain.

© 2020 Published by Elsevier.

**Low temperature synthesis of bio-fuel additives via valorisation of glycerol with benzaldehyde as well as furfural over a novel sustainable catalyst, 12-tungstosilicic acid anchored to ordered cubic nano-porous MCM-48**

Anjali Patel\* and Dhruvi Pithadia

Polyoxometalates and Catalysis Laboratory, Department of Chemistry, Faculty of Science.  
The Maharaja Sayajirao University of Baroda. Vadodara-390002. Gujarat. India.

\*E-mail: [anjali.patel-chem@msubaroda.ac.in](mailto:anjali.patel-chem@msubaroda.ac.in)

ORCID: 0000-0003-0177-3956\*

**Graphical abstract**



**Highlights**

- New heterogeneous catalyst comprising nano-porous MCM-48 & 12-tungstosilicic acid
- Solvent-free acetalization of glycerol with benzaldehyde & furfural at ambient reaction conditions
- Synthesis of dioxane derivatives with > 85 % conversion and > 60 % selectivity with high TON

## Abstract

The present article demonstrates designing of novel catalyst, 12-tungstosilicic acid (TSA) anchored to ordered nano-porous MCM-48 (nMCM-48); TSA/nMCM-48, characterization and evaluation for synthesis of bio-fuel additives via glycerol valorisation with aromatic aldehydes. The nanopores of support were confirmed by BET and TEM while the interaction between TSA and nMCM-48 was confirmed by decrease in the surface area and pore volume of the catalysts. Assessment of vital reaction parameters (% loading of active species, mole ratio of reactants, catalyst amount, temperature and time) were performed to achieve maximum conversion of glycerol. The catalyst showed noteworthy performance at 30 °C towards conversion (>85 %) and thermodynamically stable dioxane derivative (>60 %) with remarkable TON (5945 for benzaldehyde and 7355 for furfural). The catalyst was regenerated and used for successive four catalytic runs with almost same activity. The superiority of novel catalyst is because of its geometry and nano porosity.

## Keywords

Bio-fuel additives; Glycerol; Valorisation; Acetalization; Heterogeneous catalyst; High TON.

## 1. Introduction

The never-ending demand of energy supplements has geared the sudden urge of replacing non-renewable fossil fuels by renewable ones. As a result of this, the breakthrough comes from the utilization of renewable feedstock, converting into valuable chemicals, bio-additives, biodiesel and biofuels. Hence, from last two decades, there has been an unparalleled revolution in biodiesel industries producing surplus glycerol as by-product [1,2]. Collectively, up to date, these industries are unable to exploit all the glycerol formed from biodiesel manufacturing

units. Henceforth in present situation it is important to highlight the economic utilization of spare glycerol by other alternatives. In a view of upgrading glycerol at marketed level, valorisation is the best way that can be carried out via dehydration [3], hydrogenation [4], etherification [5], hydrogenolysis [6] and others [7], especially by reacting three hydroxyl groups through acetalization reaction.

Glyceryl acetals and ketals, potential biodiesel additives/blends [8,9], can be formed by condensation of glycerol with simple aldehydes & ketone using acid catalysts. Acetalization of glycerol with benzaldehyde yields isomeric products, 1,3-dioxolane (5-membered) and 1,3-dioxane (6-membered). They are important precursors to produce green platform chemicals, 1,3-propanediol and 1,3-dihydroxyacetone [10]. They have tremendous contribution as antiknock additives, excellent antioxidants and accelerators for ignition fuel, as fragrances, as food additives, in beverage, lacquer industries and pharmaceuticals [9].

According to the recent forecast data reported by International Energy Agency (Iea), in 2019, biofuel production for transport has extended 6% reaching to 96 Mtoe (161 billion litres) year-on-year and over the next five years 3% annual production growth is expected. (Figure 1) [11]. Thus, from the viewpoint of economic demands for clearing environmental sewage and adverse ecological impact along with traditional disadvantages of homogeneous catalysts, the new generation acetalization reactions via heterogeneous catalytic approach has gained tremendous attention for maximum conversion of glycerol to selective acetals/ketals.

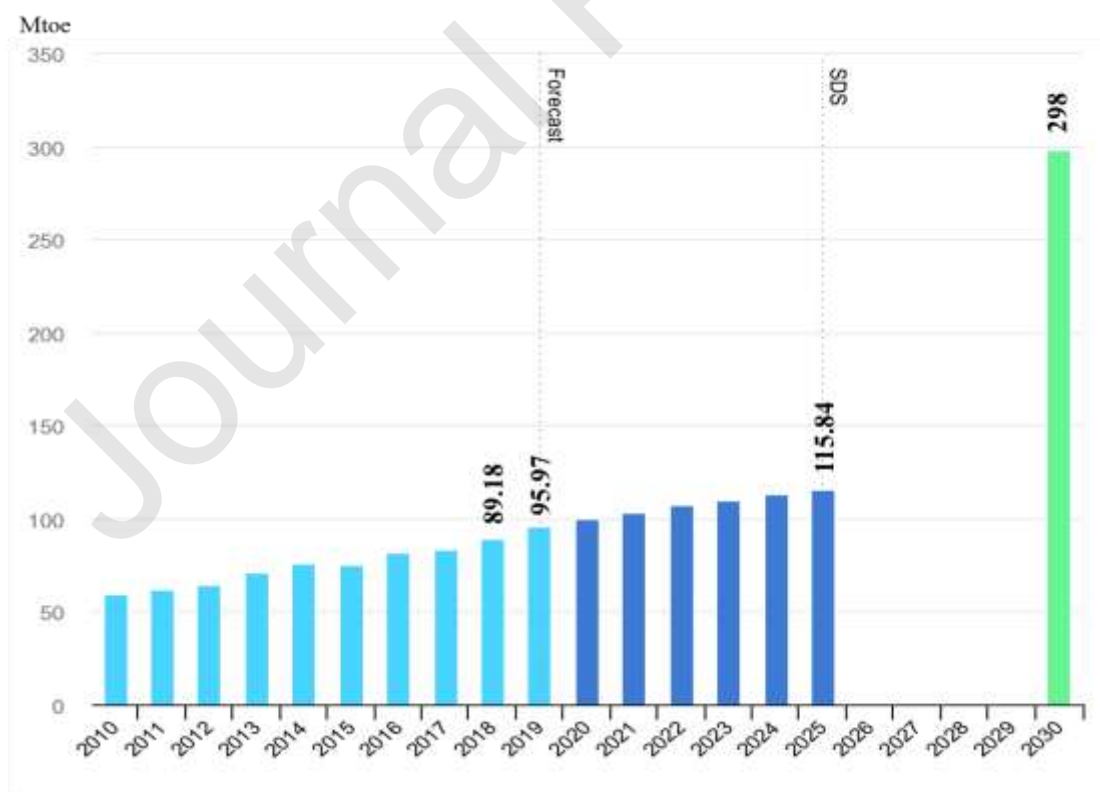


**Figure 1** Global biofuel production 2010-2025 compared to consumption in the Sustainable development Scenario [IEA (2019), Tracking Transport, IEA, Paris <https://www.iea.org/reports/tracking-transport-2019>]

Several solid acid catalysts such as, metal-based catalysts [12,13], montmorillonite [14], activated carbon [15], ion exchange resins [16], mesoporous silicates [17-19] and heteropoly acids [2,20-29] have been applied for the same. Amongst all, the contribution from heteropoly acids (HPAs) based catalysts, especially Keggin type, are found to be excellent from the viewpoint of their compositions and varied structural properties. Keggin type of HPAs are Bronsted acids, having metal-oxygen octahedra with general formula  $[XM_{12}O_{40}]^{n-}$ , where X is the heteroatom (P or Si) and M is the addenda atom (Mo, W, V etc). Sufficient illustrations for acetalization of glycerol using 12-tungstophosphoric acid are available in an art [19, 21, 22, 24, 25, 28]. Literature survey shows that, even though, TSA is the second most acidic in the HPAs series, only two reports are available, [23, 27] for the same. It is also observed that, no reports are available for acetalization of glycerol with furfural, another important industrial reaction, using anchored TSA.

Keeping in mind the importance of TSA as well as glycerol valorisation, we came with a novel heterogeneous catalyst comprising of TSA and nMCM-48. Both, support (nMCM-48) and catalyst (TSA/nMCM-48) were characterized by physicochemical/spectral techniques and evaluated for valorisation of glycerol. Essential reaction parameters (mole ratio of glycerol: benzaldehyde/furfural, catalyst amount, reaction temperature and reaction time) were screened and optimised to obtain maximum conversion and selectivity towards desired product. The catalyst was recovered by simple centrifugation and reused up to 3 cycles. The regenerated catalyst was characterized by acidity, FT-IR and BET surface area measurements to confirm its sustainability. A comparison with the reported catalysts was also carried out and correlated with nano porosity as well as geometry.

## 2. Experimental

### 2.1. Materials

All chemicals used were of A.R. grade. 12-tungstosilicic acid, liquor ammonia, TEOS (tetraethylorthosilicate), benzaldehyde, furfural, ethanol and 2-propanol were used as received from Merck. CTAB (Cetyltrimethylammonium bromide) was purchased from Loba chemie and glycerol was acquired from Suvidhinath Laboratories (SULAB; Vadodara, Gujarat).

### 2.2. Synthesis of the catalyst

The synthesis of TSA anchored to nMCM-48 was carried out in two steps.

#### *Step-I: Synthesis of nMCM-48*

The synthesis of nMCM-48 was carried out, by following the reported method with some modification [30]. To 50 g of distilled water, CTAB surfactant (2.4 g, 6.6 mmol) was added and allowed to dissolve completely at 35 °C. To this solution, ethanol (50 ml, 0.87 mmol) and 25 % wt liquor ammonia (~15.4 ml, 0.225 mol) was added and stirred for 15-20 mins, following dropwise addition of TEOS (3.4 g, 16 mmol). The resulting white suspension was aged for 2 h, filtered and washed with distilled water, dried at room temperature and calcined at 550 °C for 6 h. The material obtained was designated as nMCM-48.

*Step-II: Synthesis of the TSA anchored to nMCM-48*

A series of catalysts containing 10-40 % of TSA anchored to nMCM-48 were synthesized by wet impregnation method. 1 g of nMCM-48 was impregnated with an aqueous solution of TSA (0.1 g/ 10 mL – 0.4 g/ 40 mL of double distilled water) and dried at 100 °C for 10 h. The obtained catalysts were designated as TSA<sub>1</sub>/nMCM-48, TSA<sub>2</sub>/nMCM-48, TSA<sub>3</sub>/nMCM-48, and TSA<sub>4</sub>/nMCM-48, respectively.

### 2.3. Characterization

#### 2.3.1. Determination of total acidity, acidic strength and sites

Acidic properties of synthesized support and catalysts were determined by n-butylamine titration, potentiometric titration method and temperature programmed desorption of ammonia (NH<sub>3</sub>-TPD).

*n-butylamine titration.* For determining total acidity, n-butylamine titration method was performed. 0.25 g of support/catalyst was suspended for 24 h in 25 ml of 0.025 N n-butylamine solution in toluene. The excess base was then titrated against 0.025 N trichloroacetic acid solution in toluene using neutral red indicator to obtain total acidity of the material.

*Potentiometric titration.* To a suspension of 0.25 g of the support/catalyst in 25 mL of acetonitrile, 0.1 mL of 0.05 N, n-butylamine in acetonitrile was added and stirred at 25 °C for 3 h. Then, the suspension was titrated potentiometrically against 0.05 N solution of n-butylamine in acetonitrile. Variation in electrode potential was measured with a digital pH meter.

*NH<sub>3</sub>-TPD.* The temperature-programmed desorption (TPD) of NH<sub>3</sub> was measured on BELCAT-II (Japan) instrument. 0.05 g of dry material was loaded and allowed to pre-treat at 300 °C for 1 h in presence of pure He gas (99.9%, 30 mL per min). Ammonia (10% NH<sub>3</sub> in He gas) was adsorbed on the surface of material for 1 h and then the physisorbed ammonia was removed by flushing with pure He gas. Finally, the temperature programmed was performed from 100 to 600 °C with a ramp rate of 10 °C/min. Desorbed NH<sub>3</sub> was monitored by using TCD (thermal conductivity detector) of the apparatus.

### 2.3.2. Physicochemical techniques

Elemental analysis was carried out using JSM-7100F EDX-SEM analyser. Thermogravimetric analysis (TGA) of synthesized support/catalyst was performed using a Mettler Toledo Star SW 7.01 instrument under nitrogen atmosphere in the temperature range of 50–800 °C with flow rate of 2 mL min<sup>-1</sup> and with heating rate of 10 °C min<sup>-1</sup>. For FT-IR spectra, the samples were compelled with dry KBr into discs and recorded in the range of wave numbers 4000-400 cm<sup>-1</sup> by using Shimadzu instrument (IRAffinity-1S). The BET surface area measurements were performed in a Micromeritics ASAP 2010 volumetric static adsorption instrument with N<sub>2</sub> adsorption at 77 K. The pore size distributions were calculated by BJH adsorption-desorption method. Scanning electron microscope (SEM) images were recorded on JSM-7100F scanning electron microscope. Transmission electron microscopy (TEM) was performed on JEOL TEM instrument (model-JEM 2100) by applying acceleration voltage of 200 kV using carbon coated 200 mesh Cu grid. The samples were dispersed by ultrasonication and coated on grid, leaving overnight for drying in air. The X-ray powder diffraction (XRD) patterns of the support and the catalyst were measured using a D8 FOCUS X-ray Diffractometer from Bruker in the 2θ range of 0-80° using CuKα radiation ( $\lambda = 1.54056 \text{ \AA}$ ). <sup>29</sup>Si MAS NMR was recorded using JOEL ECX 400 MHz High resolution multinuclear FT-NMR spectrometer for solids.

### 2.4. Catalytic evaluation

The acetalization of glycerol was carried out in 50 mL 2 neck glass reactor under nitrogen atmosphere. The reactor was charged with glycerol (0.01 mol), benzaldehyde (0.01 mol) / furfural (0.01 mol) and catalyst. The reaction mixture was stirred vigorously at 30 °C under N<sub>2</sub> atmosphere, followed by diluting the contents with 2-propanol and analysed using Shimadzu 2014 GC equipped with RTX-5 capillary column (internal diameter: 0.25 mm, length: 30 m). The products were identified by GC-MS (Gas chromatography-mass spectrometry- Thermo scientific DSQ-II; Capillary column- Thermo TR-MS).

Turnover number (TON) refers to the moles of product formed per mole of catalyst. It was calculated by using the following formula:

$$\text{TON} = \frac{\text{number of moles of product}}{\text{number of moles of catalyst}}$$

Number of moles of catalyst was calculated by taking the amount of TSA incorporated.

### 2.5. Leaching test

Escape of any active species from the support makes the catalyst unappealing and hence it is mandatory to analyse leaching of TSA from nMCM-48. Heteropoly acids can be determined

qualitatively via heteropoly blue colour, when treated with mild reducing agent like ascorbic acid. To check the leaching of any TSA from the support, suspension of 1 g of catalyst with 10 ml conductivity water was allowed to reflux for 24 h. The resulting supernatant solution was treated with 10 % ascorbic acid solution and the absence of blue colour indicates no leaching of TSA. The similar test was performed for the residue obtained after reaction completion and absence of blue colour indicates no leaching of TSA.

### 3. Results and discussion

#### 3.1. Catalyst Characterization

The effective TSA loading in all catalysts was calculated by the following equation.

$$\text{Loading amount (\%)} = \frac{\text{Weight of TSA}}{(\text{Weight of TSA}) + (\text{Weight of nMCM-48})} \times 100$$

According to the given formula, for the series of catalysts, TSA<sub>1</sub>/nMCM-48, TSA<sub>2</sub>/nMCM-48, TSA<sub>3</sub>/nMCM-48 and TSA<sub>4</sub>/nMCM-48, the subscript 1, 2, 3 and 4 indicates loading of TSA, which is 9, 16.66, 23.07 and 28.5 wt%, respectively.

The values of elemental analysis by EDX (Table 1) for all catalysts were in good agreement with theoretical calculated value of tungsten (W) except for TSA<sub>4</sub>/nMCM-48 indicating effective loading of TSA. However, it should be noted that the variation in case TSA<sub>4</sub>/nMCM-48, may be due to insufficient loading. The EDX elemental mapping of TSA<sub>3</sub>/nMCM-48 is shown in figure 2 while others are included in supplementary material (Figure S1).

**Table 1.** Elemental analysis of catalysts

Material	Si (wt%)	O (wt%)	W (wt%)	
			By EDX	Theoretical
TSA <sub>1</sub> /nMCM-48	41.34	52.19	6.48	6.96
TSA <sub>2</sub> /nMCM-48	35.96	51.46	12.58	12.7
TSA <sub>3</sub> /nMCM-48	23.73	58.93	17.34	17.7
TSA <sub>4</sub> /nMCM-48	30.59	49.28	20.13	21.8

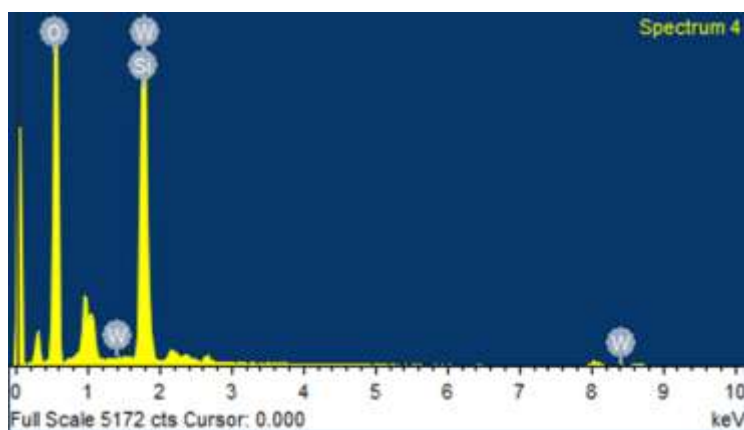


**Figure 2** EDX elemental mapping of TSA<sub>3</sub>/nMCM-48 (colour)

It is seen from Table 2 that as the amount of TSA loading increases, total acidity also increases. This may be due to enhancement in the concentration of Bronsted acidity of TSA inside nMCM-48, which is in good agreement with results of elemental analysis. However, on increasing the amount of TSA from 30 % to 40 %, no significant change in total acidity was observed. The acidic strength and total number of acidic sites of synthesized catalysts including support were determined by potentiometric titration. The acid strength of surface sites can be assigned according to the following scale:  $E_i > 100$  mV (very strong sites),  $0 < E_i < 100$  mV (strong sites),  $-100 < E_i < 0$  mV (weak sites) and  $E_i < -100$  mV (very weak sites) [28]. The plots of the electrode potential as a function of meq. n-butylamine per g of the material are shown in supplementary figure S2. From the data presented in Table 2, it is well distinct that as the amount of TSA loading on nMCM-48 increases from 10 – 30 %, the acidic strength increases significantly, while negligible change observed from 30 – 40 %. The increase in number of very strong and strong acidic sites is directly related to the amount of TSA which is attributed to enhanced Bronsted acid sites.

**Table 2.** Acidity measurements of support and catalysts

Material	Potentiometric titration			n-butylamine titration	
	Acidic strength (mV)	Types of acidic sites (meq g <sup>-1</sup> )		Total No. of acidic sites (mmol g <sup>-1</sup> )	Total acidity (mmol g <sup>-1</sup> )
		Very strong	Strong		
nMCM-48	168	0.1	2.3	0.48	1.04
TSA <sub>1</sub> /nMCM-48	646	0.3	2.3	0.52	1.28
TSA <sub>2</sub> /nMCM-48	676	0.6	2.7	0.66	1.32
TSA <sub>3</sub> /nMCM-48	700	1.4	3.5	0.98	1.44
TSA <sub>4</sub> /nMCM-48	706	1.3	3.6	1.04	1.46

Noted that only a slight increase in the acidic strength as well as the total number of acidic sites was observed from 30 % to 40 % loading of TSA, which is in good agreement with the value of total acidity. This may be due to the blocking of the sites as well as insufficient impregnation, which was also observed in the EDX analysis. Hence TSA<sub>3</sub>/nMCM-48 was considered for detailed characterization and re-coded as TSA/nMCM-48.

To confirm the types of acidic sites, the support and catalyst were further characterized by NH<sub>3</sub>-TPD analysis (Figure 3). The profile of support and the catalyst exhibits combined desorption peak for weak as well as moderate acid sites. Desorbed amount of ammonia can be directly related to the amount of the acid sites on the sample and also the strength of the acid sites can be determined by desorption temperature. NH<sub>3</sub> desorbed below 200 °C is due to weak acidic site. Around 250-400 °C, desorption occurs due to medium/moderate acidic sites and above 500 °C is due to strong acid site. It is well distinct from the figure 1 that for nMCM-48 negligible amount of ammonia was desorbed indicating presence of few weak and moderate acidic sites. After introduction of TSA, elevation of peak area from 100 -300 °C was observed corresponding to the increase in weak and moderate Bronsted acid sites [31]. Thus, the overall enhancement in the acidic sites of material was obtained due to incorporation of TSA inside the pores of nMCM-48, which is in good agreement with reported one [23].

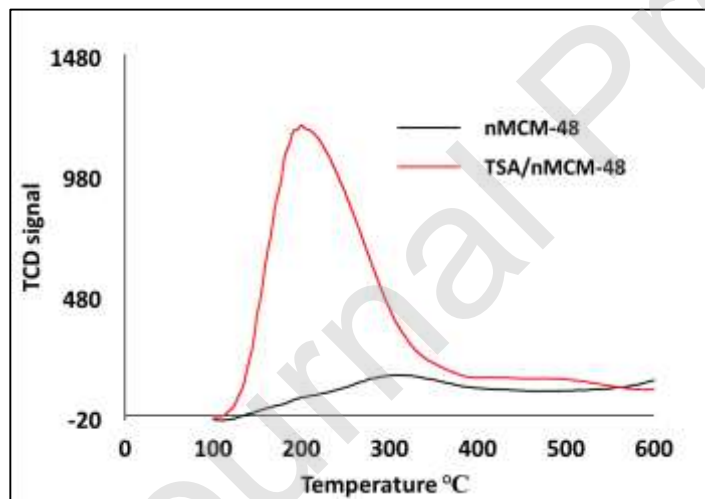


**Figure 3** NH<sub>3</sub>-TPD profile of nMCM-48 and TSA/nMCM-48 (colour)

TGA for nMCM-48 and TSA/nMCM-48 are shown in supplementary figure S3. From the plots it is seen that the weight loss occurs mainly in two stages. For nMCM-48, the initial weight loss of 8.9 % up to 110 °C may be due to the desorption of physically absorbed water molecules. Final weight loss of <1 % up to 400 °C is attributed to the condensation of silanol groups present in the nMCM-48 [32]. After that, no weight loss was observed, which indicates the stability up to 550 °C. While TSA/nMCM-48, shows initial weight loss of 8.1 % up to 115 °C corresponding

to adsorbed water. The second weight loss of 0.67 % up to 200 °C can be attributed to crystalline water molecules present in Keggin unit [23]. After that, no gradual weight loss up to 550 °C, shows the stability of the catalyst.

FT-IR spectrum (Figure 4) of pure nMCM-48 shows a broad band around 1100  $\text{cm}^{-1}$  and 1250  $\text{cm}^{-1}$  which corresponds to Si-O-Si asymmetric stretching. It also shows bands at 578 and 462  $\text{cm}^{-1}$ , which can be attributed to the symmetric stretching of Si-O-Si and bending vibration of Si-O respectively. Symmetric stretching vibration of Si-O-Si and bending vibration of Si-O are depicted by the bands around 578 and 462  $\text{cm}^{-1}$  respectively. The broad band at 3448  $\text{cm}^{-1}$  is due to the absorption of hydroxyl group from presence of large amount of  $\text{H}_2\text{O}$ . The obtained bands are in good agreement with the reported one [33]. FT-IR of TSA/nMCM-48 shows two of the characteristic bands for the Keggin unit TSA at 972 and 925  $\text{cm}^{-1}$  corresponding to asymmetric vibrations of  $\text{W-O}_d$  (terminal oxygen linked to a lone tungsten atom) and  $(\text{Si-O}_a)$  respectively. Presence of these fingerprint bands directs that the primary structure of TSA is completely unchanged even after impregnation on the support.

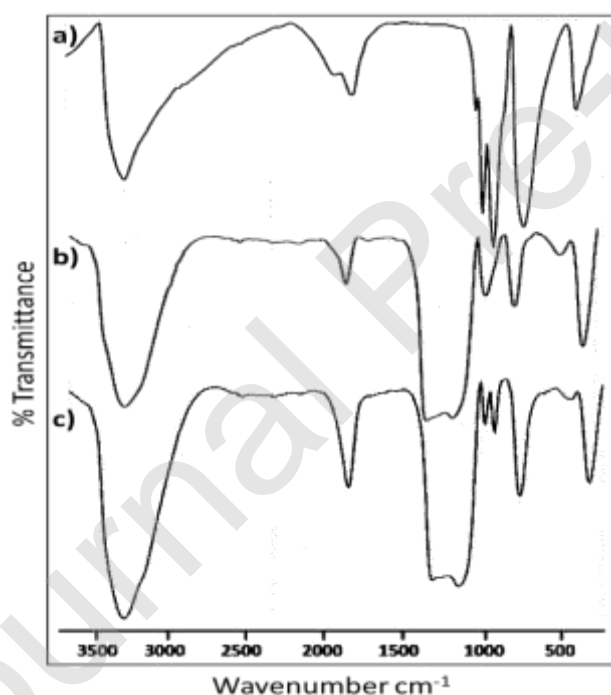


**Figure 4** FT-IR spectra of a) TSA b) nMCM-48 c) TSA/nMCM-48

The nonappearance of vibrational bands around 880  $\text{cm}^{-1}$  ( $V_{\text{as}}(\text{W-O}_b\text{-W})$ ) and 785  $\text{cm}^{-1}$  ( $V_{\text{as}}(\text{W-O}_c\text{-W})$ ) of TSA may be due to superimposition with the bands of nMCM-48 [34]. Further, FT-IR spectra of TSA/nMCM-48 also shows an additional peak at 1635  $\text{cm}^{-1}$ , may be due to the bending vibration of bridging hydroxyl groups, resulting from the hydrogen bond between terminal oxygen of TSA and hydrogen of silanol groups of nMCM-48.

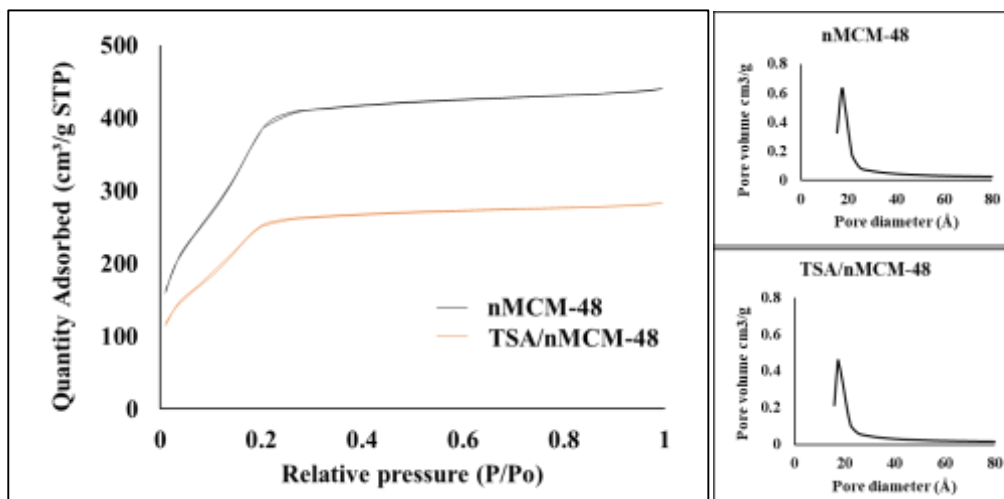
Textural properties of support as well as catalysts are shown in Table 3. Relatively small pore diameter of nMCM-48 gives the first indication that the support is nano-porous in nature with high specific surface area. Significant decrease in both, surface area as well as pore volume clearly indicate the incorporation of TSA inside the porous network of nMCM-48. It is very interesting to note down a decrease in surface area and increase in the pore value for TSA<sub>4</sub>/nMCM-48, indicating blocking of the sites because of the multilayer adsorption of TSA. Looking at the values of pore volume and pore diameter, once again, TSA<sub>3</sub>/nMCM-48 was selected for the further study.

**Table 3.** Textural properties of support and catalysts

Material	Surface area (m <sup>2</sup> /g)	Pore volume (cm <sup>3</sup> /g)	Pore diameter (Å)
nMCM-48	1307	0.63	20.8
TSA <sub>1</sub> /nMCM-48	712	0.24	20.1
TSA <sub>2</sub> /nMCM-48	637	0.25	19.2
TSA <sub>3</sub> /nMCM-48	588	0.21	18.3
TSA <sub>4</sub> /nMCM-48	333	0.23	17.8

\*TSA<sub>3</sub>/nMCM-48 = TSA/nMCM-48

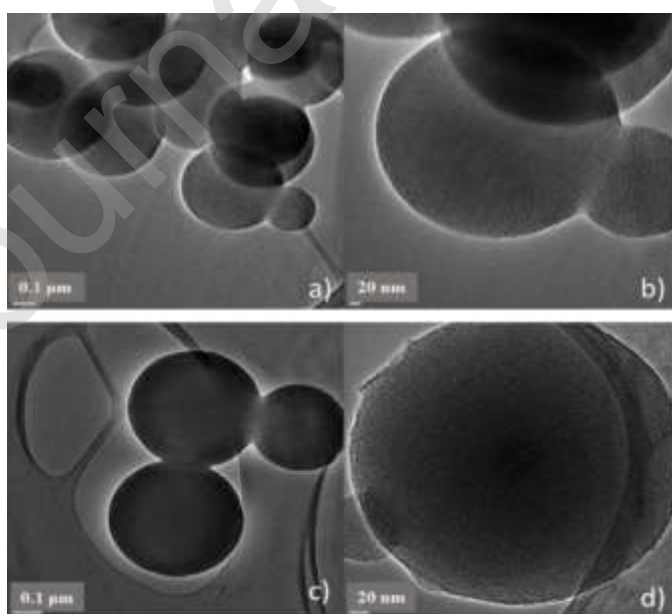
The N<sub>2</sub> adsorption-desorption isotherms of nMCM-48 and TSA/nMCM-48 (Figure 5) shows typical nature of type IV(b), conforming the formation of mesoporous structure. According to the IUPAC technical report, capillary condensation for the pores having smaller width are completely reversible with the absence of a hysteresis loop. In the present case, the obtained completely reversible isotherms are without hysteresis loop indicating the smaller width and confirming the nano-porous structure. The observation is in good agreement with the reported one [35]. The uniformity in the size of nanopores is well distinct from the sharpness of the step and position of the inflection point which is related to the diameter of pores (20.8 Å). For nMCM-48, adsorption in the mesopores is well distinct in the range of relative pressure between 0.2 - 0.3 which disappears for TSA/nMCM-48 indicating the effective filling of mesopores by TSA [36].



**Figure 5** Nitrogen ( $N_2$ ) adsorption-desorption isotherms (colour)

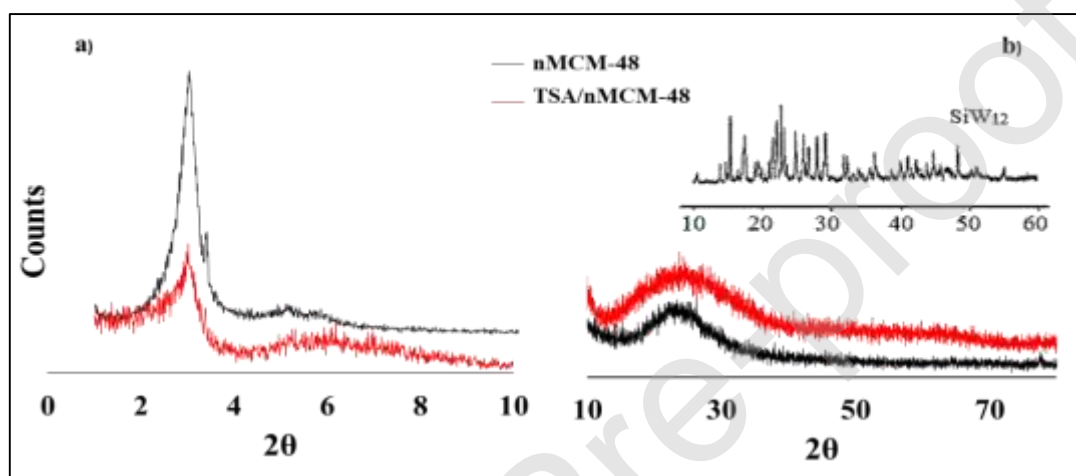
SEM images (supplementary figure S4) shows spherical morphology with a uniform particle size of nMCM-48. SEM micrograph of TSA/nMCM-48 indicates the homogeneous distribution of spheres and there is no noticeable change observed in the morphology even after the introduction of TSA species, indicating its fine dispersion into three dimensional pores, further confirmed by XRD.

TEM images (Figure 6) of nMCM-48 and TSA/nMCM-48 were recorded at various magnifications. Figure 6a & 6b of nMCM-48 shows well-ordered pore networks with uniform particle diameter, confirming the nano-porous structure, which is in good agreement with the BET surface area analysis. Opaque spheres were observed in TSA/nMCM-48 (Figure 3c & 3d), where the maximum pores are uniformly filled with TSA. This is further confirmed by XRD.



**Figure 6** TEM images of a, b) nMCM-48 c, d) TSA/nMCM-48

The Low angle powder XRD analysis (Figure 7a) shows a typical pattern of nMCM-48 exhibiting characteristic diffraction peaks at  $3.0^\circ$  and  $3.36^\circ$   $2\theta$  corresponding to the plane 211 and 220, respectively. In the range of  $4 - 5^\circ$   $2\theta$ , numerous peaks correspond to the reflection planes 400, 321 and 420 of MCM-48 having Ia3d cubic symmetry [37]. The XRD pattern of TSA/nMCM-48 depicts the decrease in intensity of characteristic peak with slight broadening which is in good agreement with the reported one [38]. Wide angle XRD pattern (Figure 7b) of anchored MCM-48 shows the absence of characteristic peaks of the crystalline phase of TSA, signifying very fine dispersion of it into the pores of nMCM-48 [39]. Collectively, it can be inferred from the XRD results, that the structure of nMCM-48 remains intact even after impregnation of TSA.

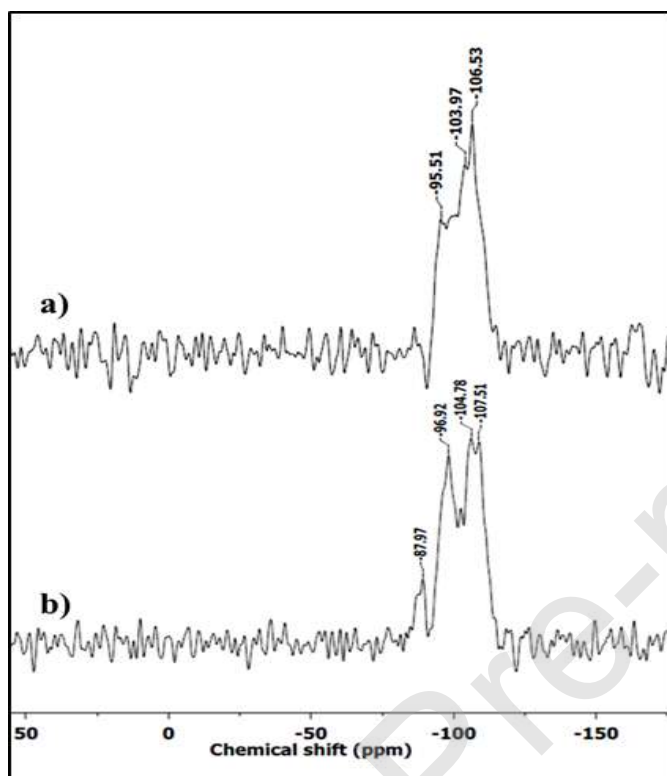


**Figure 7** a) Low angle Powder XRD patterns b) Wide angle Powder XRD patterns (colour)

To identify the interactions between of nMCM-48 and TSA, solid state  $^{29}\text{Si}$  MAS-NMR was performed. Typical broad peak for nMCM-48 was observed between  $-95$  and  $-120$  ppm corresponding to the three main components  $Q^2$ ,  $Q^3$  and  $Q^4$  (Figure 8). The notation  $Q^x$  describes the number of  $x$  siloxane linkages to a silicon atom. For instance, the  $Q^2$  signal corresponds to the disilanol linkage  $\text{Si}(\text{O}-\text{Si})_2(\text{O}-\text{X})_2$ , where  $X$  is  $\text{H}$  or  $\text{TSA}$ . Similarly, resonating peaks for  $(\text{O}-\text{X})-\text{Si}(\text{O}-\text{Si})_3$  and  $\text{Si}(\text{O}-\text{Si})_4$  corresponds to  $Q^3$  and  $Q^4$  respectively. The chemical shift values for all components are mentioned in table 3. The observed values of chemical shifts for nMCM-48 are in good agreement with the reported literature [40]. The observed minor downfield shift in the value of chemical shift for  $Q^2$ ,  $Q^3$  and  $Q^4$  as well as broadening in the spectrum of TSA/nMCM-48 as compared to n MCM-48 may be due to the presence of TSA. Also, a slight change in the intensities of  $Q^2$  and  $Q^3$  peaks were observed, indicating the strong bonding of TSA to proton of silanol groups of nMCM-48. Evidently, the signal for TSA appears in the range of  $-81$  to  $-90$  ppm, which is depicted in the spectrum at  $-87.97$  ppm, showcasing the unchanged Keggin structure of TSA. [41].

**Table 4.**  $^{29}\text{Si}$  chemical shifts of nMCM-48 and TSA/nMCM-48

Material	Si nuclei ppm (TSA)	Q <sup>2</sup> ppm	Q <sup>3</sup> ppm	Q <sup>4</sup> ppm
nMCM-48	-	-95.51	-103.97	-106.53
TSA/nMCM-48	-87.97	-96.92	-104.78	-107.51

**Figure 8**  $^{29}\text{Si}$  MAS NMR spectra of a) nMCM-48 b) TSA/nMCM-48

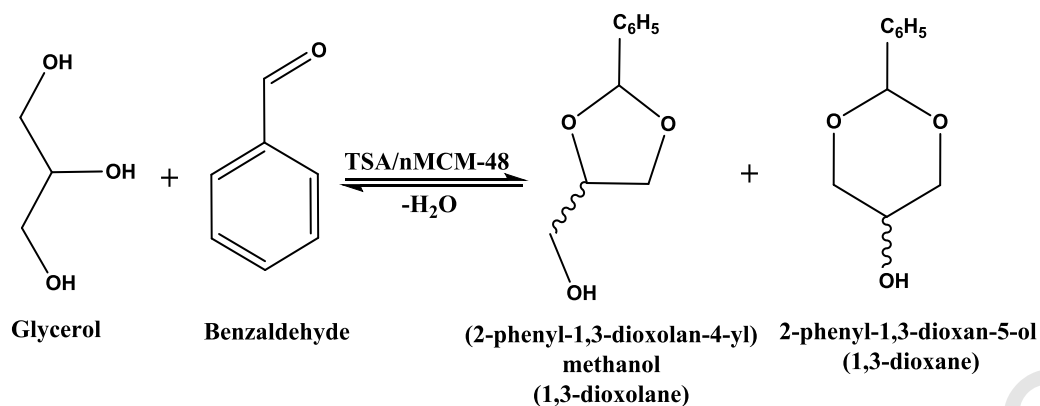
Thus, acidity measurements show that the total acidity as well as acidic strength increases after the introduction of TSA into nMCM-48. BET and FT-IR studies indicates the inclusion of undegraded TSA into the nanopores of nMCM-48 via hydrogen bonding between terminal oxygen and hydrogen of silanol groups of nMCM-48. TEM, XRD and  $^{29}\text{Si}$  MAS NMR confirm the meso structure with nanopores, fine dispersion of TSA inside nMCM-48 and strong interaction of silanol groups to TSA inside pores of nMCM-48, respectively.

### 3.2. Catalytic evaluation

#### 3.2.1 Acetalization of glycerol with benzaldehyde

Glycerol acetalization with benzaldehyde yields two cyclic products, 1,3-dioxolane (5-membered) and 1,3 dioxane (6- membered) (Scheme-1), amongst which 1,3-dioxane is thermodynamically favoured. To study the effect of % loading of TSA, reactions were carried using 10, 20, 30 and 40 % TSA loaded nMCM-48. From figure 9a, it is seen that as the % of

TSA increases, % conversion also increases from 67 to 98 %. However, the trend does not show a significant change in conversion from 30 to 40 % loading. Hence, considering the equivalent effect in terms of acidity measurements as well as % conversion, the catalyst with 30 % TSA loading, TSA/nMCM-48 was selected for the detailed study.



**Scheme 1** Acetalization of glycerol with benzaldehyde

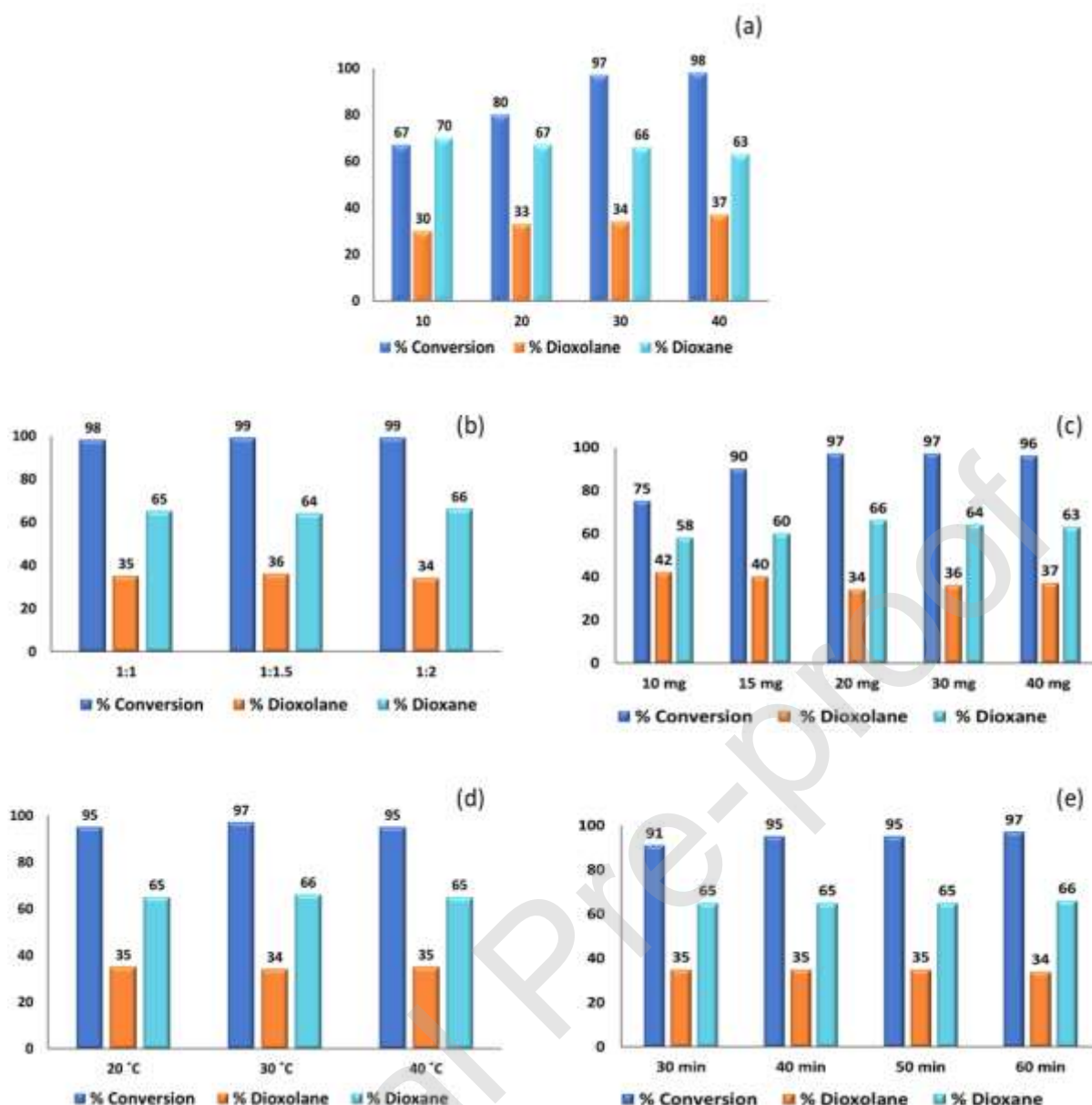


**Figure 9.** (a) Effect of % loading TSA. Mole ratio: 1:1; Catalyst amount: 50 mg; Temperature: 30 °C; Time: 60 min; (b) Effect of mole ratio. Catalyst amount: 50 mg; Temperature: 30 °C; Time: 60 min; (c) Effect of catalyst amount. Mole ratio: 1:1; Temperature: 30 °C; Time: 60 min; (d) Effect of reaction temperature. Mole ratio: 1:1; Catalyst amount: 20 mg; Time: 60 min; (e) Effect of reaction time. Mole ratio: 1:1; Catalyst amount: 20 mg; Temperature: 30 °C (colour)

The effect of mole ratio of glycerol to benzaldehyde was studied by varying from 1:1 to 1:2 (Figure 9b). 98 % glycerol conversion with 65 % and 35 % selectivity of 1,3-dioxane and 1,3-dioxolane respectively, was obtained with 1:1 mole ratio. By increasing the ratio to 1: 1.5 and 1: 2, there was no significant change in the conversion of glycerol and selectivity. As a result, 1:1 mole ratio was considered optimum for further catalytic evaluation. The initial feasibility of the catalyst indicates the selective formation of thermodynamically stable 1,3- dioxane (six membered acetal) and hence further parameters were optimised by focusing the selectivity for the same.

The effect of catalyst amount was studied by screening the range 10 - 50 mg (Figure 9c). Initially, from 10 mg to 20 mg marginal increase in the % conversion was observed. Further increase in catalyst amount did not show any significant effect in terms of conversion as well as selectivity. The observed behaviour is may be due to the blocking of sites/ saturation of the number of active sites available vs. reactant amount. Hence, 20 mg was considered to be optimum amount.

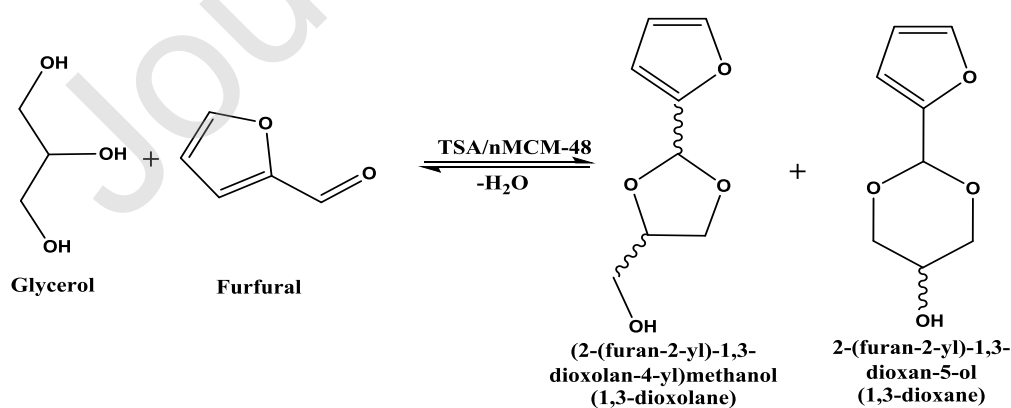
The most important parameter which governs the equilibrium of reaction is the reaction temperature. It is well-known that acetalization reaction has low equilibrium constant and is exothermic in nature [16]. Screening of reaction temperature ranging from 20 to 40 °C over TSA/MCM-48 was carried out. As depicted by the plot in figure 9d, there was no major rise in the % conversion and selectivity of desired thermodynamically stable product, hence, an easily accessible temperature, 30 °C was optimized for the said conversion.

From figure 9e it is seen that % conversion increased from 30 to 40 min, with no change in the selectivity of products. Despite increasing the reaction time from 40 to 60 min, very negligible rise of 2 % in glycerol conversion was observed which indicates the establishment of equilibrium beyond 40 min. Thus, 40 min was considered to be optimum time for reaction.

The optimised reaction conditions for the maximum conversion of glycerol (95 %) and selectivity of dioxane (65 %) are: glycerol: benzaldehyde w/w ratio 1: 1; catalyst amount 20 mg; active amount of TSA 4.6 mg; substrate: catalyst ratio (mol: mol) 6257:1; reaction temperature 30 °C; reaction time 40 min with TON 5945.

### 3.2.2. Acetalization of glycerol with furfural

In order to evaluate efficiency and versatility of catalyst, reaction with heterocyclic aldehyde-furfural (Scheme 2) was also studied by varying the same parameters as mentioned for benzaldehyde and the obtained results are presented in Figure 10.



**Scheme 2** Acetalization of glycerol with furfural

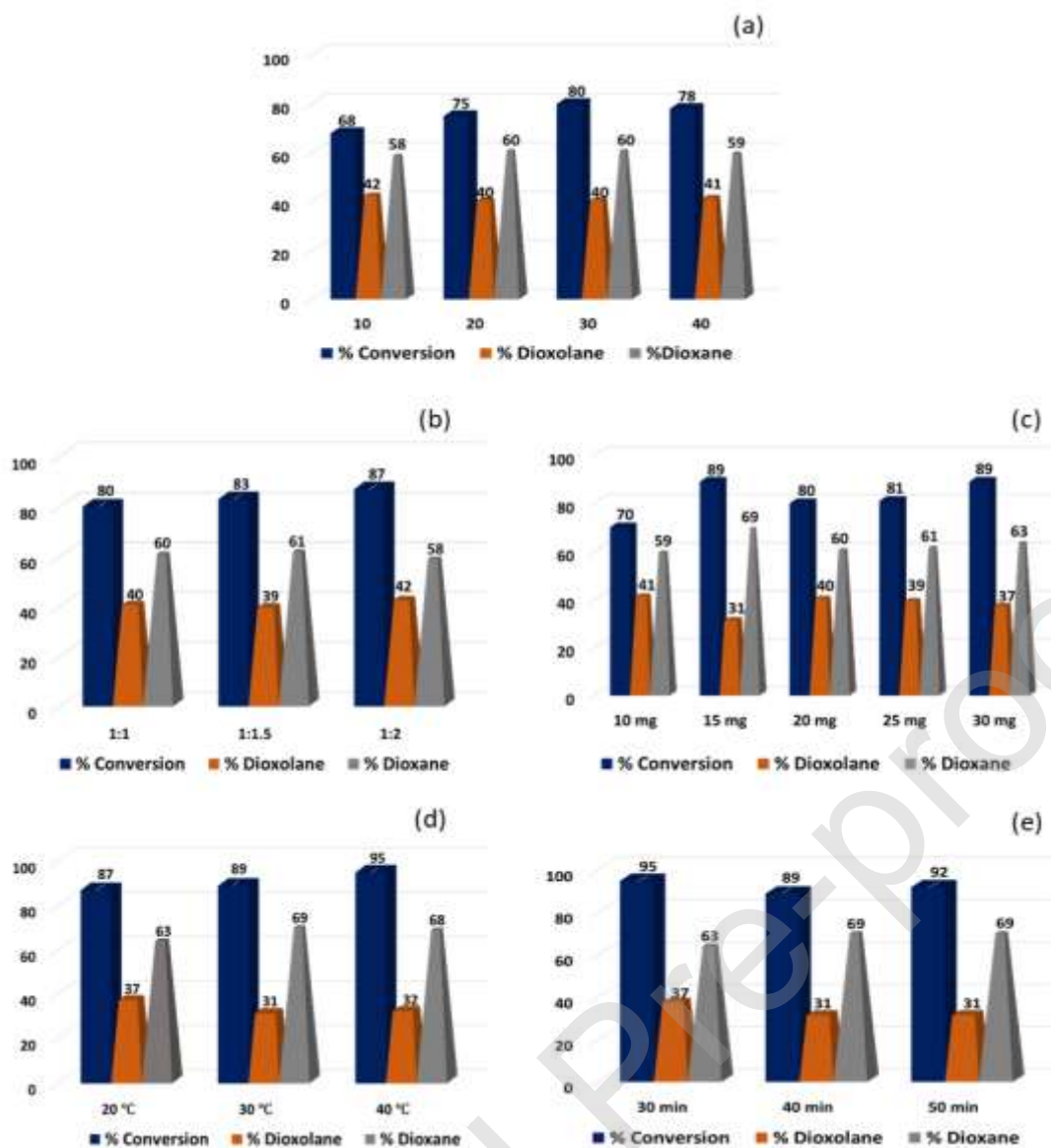


**Figure 10** (a) Effect of % loading TSA. Catalyst amount: 20 mg; Temperature: 30 °C; Time: 40 min; (b) Effect of mole ratio. Catalyst amount: 20 mg; Temperature: 30 °C; Time: 40 min; (c) Effect of catalyst amount. Mole ratio: 1:1; Temperature: 30 °C; Time: 40 min; (d) Effect of reaction temperature. Mole ratio: 1:1; Catalyst amount: 15 mg; Time: 40 min (e) Effect of reaction time. Mole ratio: 1:1; Catalyst amount: 15 mg; Temperature: 30 °C (Colour)

The optimum conditions for glycerol acetalization with furfural for maximum conversion (89 %) and selectivity (69 %) towards dioxane are: glycerol: furfural w/w ratio 1:1; catalyst amount 15 mg; active amount of TSA 3.5 mg; substrate: catalyst ratio (mol: mol) 8223:1; reaction temperature 30 °C; time 40 min with TON 7355. Requirement of low catalyst amount (15 mg) can be due to the presence of active furan ring in furfural.

### 3.3. Kinetics: Determination of activation energy

For determining the activation energy, both the reactions were subjected to different time intervals at 20, 30 and 40 °C, keeping the other parameters same as in optimised reaction condition and the obtained rate constants (k) are presented in table 5. Using these data, the value of activation energy (Ea) was calculated from the slope of graph (ln k vs 1/T, K<sup>-1</sup>) (Figure 11) by Arrhenius equation.

Table 5. Kinetic parameter (k min<sup>-1</sup>) at different temperatures and activation energy (Ea)

Temperature (K)	Glycerol with Benzaldehyde		Glycerol with Furfural	
	Rate constant k (min <sup>-1</sup> )	Activation energy Ea (kJ/mol)	Rate constant k (min <sup>-1</sup> )	Activation energy Ea (kJ/mol)
293	1.512 x 10 <sup>-2</sup>		1.85 x 10 <sup>-2</sup>	
303	4.032 x 10 <sup>-2</sup>	43	2.55 x 10 <sup>-2</sup>	36
313	4.680 x 10 <sup>-2</sup>		4.73 x 10 <sup>-2</sup>	

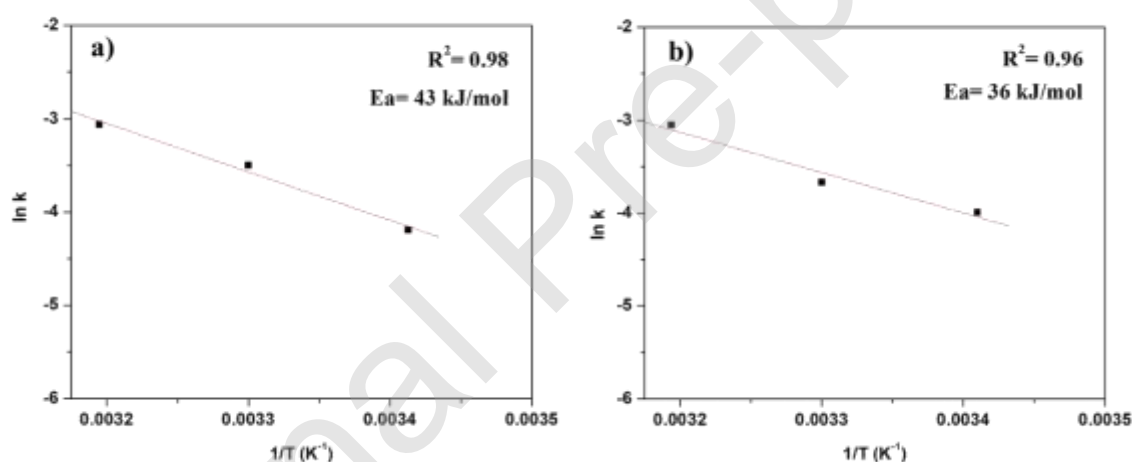


**Figure 11** Plot for determination of activation energy (ln k vs 1/T, K<sup>-1</sup>) a) Glycerol acetalization with benzaldehyde b) Glycerol acetalization with furfural

It is reported in the literature that for the reactions following diffusion regime, the activation energy is as low as 10-15 kJ/mol, while for the reactions governed by truly chemical step, the activation energy is greater than 25 kJ/mol [42]. Here, in both the cases, the activation energy is exceeding 25 kJ/mole, which clearly suggests that the reactions are governed truly by chemical step.

It is interesting to note that the activation energy for the acetalization of glycerol with furfural (36 kJ/mol) is lower as compared to that with benzaldehyde (43 kJ/mol). The values of activation energy clearly indicate that the lower activation energy for furfural can be attributed

to the presence of active furan ring which requires comparatively less prompt effect for the reaction to proceed in forward direction.

### 3.4. Control experiments

The control experiments for acetalization of glycerol with benzaldehyde and furfural were performed in their respective optimised reaction conditions. From the results demonstrated in Table 6, it was observed that the support alone is not active for the desired transformations and almost similar activity was seen for TSA and TSA/nMCM-48. This confirms that the reactivity is only due to the active keggin unit, TSA, present inside the porous framework and it can be attributed to successful anchoring of TSA. Hence, we have fruitfully synthesized a catalyst which is truly heterogeneous in nature.

**Table 6.** Control experiments

Catalysts	Glycerol with Benzaldehyde <sup>a</sup>		Glycerol with Furfural <sup>b</sup>	
	% Conversion	% selectivity of Dioxane	% Conversion	% selectivity of Dioxane
nMCM-48	1.5	49	3.1	52
TSA	97	62	91	58
TSA/nMCM-48	95	65	89	69

Reaction conditions: Mole ratio 1:1, reaction temperature, reaction time: 40 min, amount of nMCM-48 <sup>a</sup>15.4 mg, <sup>b</sup>11.5 mg, amount of TSA <sup>a</sup>4.6 mg, <sup>b</sup>3.5 mg, catalyst amount <sup>a</sup>20 mg, <sup>b</sup> 15 mg

### 3.5. Recycling studies

To reduce the overall cost of production, feasibility of heterogeneous catalyst can be determined by its recycling. For recycling studies, the catalyst was collected by centrifugation after reaction completion and simply treated with methanol to remove the substrate and product remains from the surface, followed by water wash. The catalyst was dried at 100 °C and reused for the next catalytic run. The result (Figure 12) shows that the catalyst is stable without any leaching of TSA during the reaction.

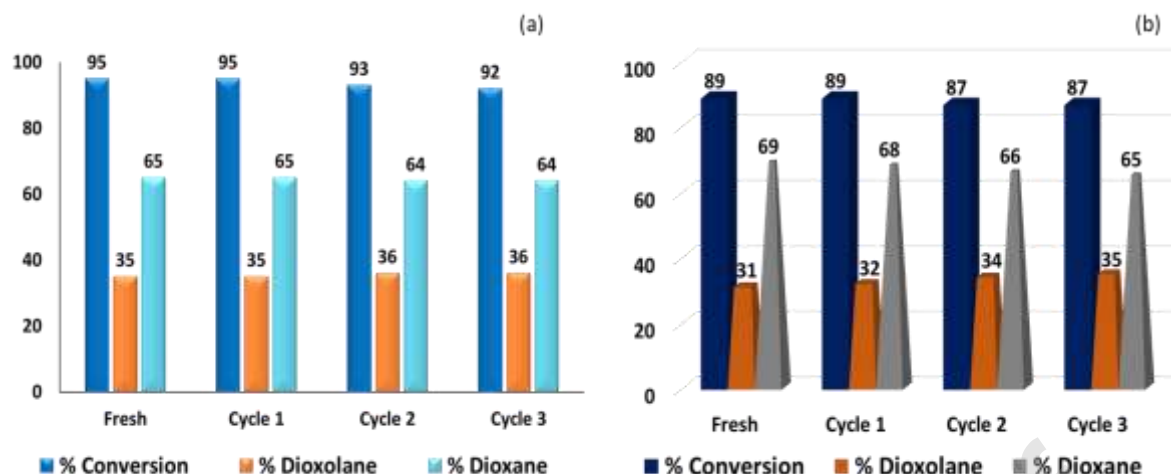


Figure 12 (a) Reaction conditions: Mole ratio (Glycerol: Benzaldehyde) 1:1; Catalyst amount: 20 mg; Temperature: 30 °C; Time: 40 min

(b) Reaction conditions: Mole ratio (Glycerol: Furfural) 1:1; Catalyst amount: 15 mg; Temperature: 30 °C; Time: 40 min (**colour**)

### 3.6. Characterization of regenerated catalyst

In order to check sustainability, the regenerated catalyst was characterized by n-butyl amine titration, BET surface area and FT-IR analysis. Total acidity obtained by n-butyl amine titration method for regenerated catalyst ( $1.43 \text{ mmol g}^{-1}$ ) was in good agreement with that of fresh one ( $1.44 \text{ mmol g}^{-1}$ ), indicating the unaltered acidic property of catalyst. The  $\text{N}_2$  adsorption-desorption isotherms (Supplementary figure S5a) of fresh and regenerated catalyst shows identical curves with no change in BET surface area,  $588$  &  $580 \text{ m}^2/\text{g}$  respectively. This also suggests that there is no alteration in the structure of catalyst after reaction. In FT-IR analysis (Supplementary figure S5b), presence of all the characteristic bands in spectra with no shifting of values, confirms that there is no leaching and change in the structure of keggin unit. However, a little bit of decrease in intensity of FT-IR bands was observed due to the regeneration process.

### 3.7. Effect of nature of substrates

To study the relative reactivity of benzaldehyde and furfural in presence of synthesized catalyst, reactions were carried in same experimental conditions and obtained results are presented in table 7. It is interesting to note from the results that simple aromatic aldehyde, benzaldehyde requires more catalyst amount than heterocyclic aldehyde, furfural for maximum conversion and selectivity. This can be attributed to the presence of active furan ring in furfural which proceeds to form acetals more dominantly than benzaldehyde. This observation is in good agreement with the obtained values of activation energy, where formation of acetals of

furfural shows comparatively lower activation energy than that for acetals of benzaldehyde. Also, in case of furfural increase in catalyst amount (20 mg) decreases the conversion (80 %) as well as selectivity (60 %) (Figure 10c) which may be due to the mass density increase and less available surface sites for catalytic reaction. Hence, it can be inferred that heterocyclic aldehydes requires a less trigger effect from the acid catalyst to readily form acetals at ambient reaction conditions.

**Table 7.** Effect of nature of substrates

Substrate	% Conversion	% selectivity of Dioxane	TON
Benzaldehyde	88	60	7272
Furfural	89	69	7355

Reaction conditions: mole ratio 1:1, reaction temperature 30 °C; reaction time 40 min; catalyst amount: 15 mg; active amount of TSA 3.5 mg

### 3.8. Comparison with the reported catalysts

For the present catalyst, catalytic activities for both the reactions are compared with the reported ones, considering the conversion based on glycerol and focusing on selectivity of dioxane derivative.

As seen in table 8, in case of benzaldehyde, the advantage of present catalyst lies in the best glycerol conversion (95 %) as well as selectivity towards dioxane compared to the reported catalysts. Similarly, for furfural, highest conversion (89 %) as well as double the dioxane selectivity (69 %) is obtained compared to the reported ones. It is interesting to note that while the reported systems have been carried out under comparatively harsher conditions, the present catalyst is highly effective and greener in terms of very less catalyst amount, lower temperature, less reaction time and solvent free condition. The superior activity of the present catalyst can be attributed to the unique acidity of TSA as well as 3D cubic geometry and nano porosity of support which enables the formation of thermodynamically stable derivative at ambient conditions.

**Table 8.** Comparison with reported catalysts

<b>Glycerol with benzaldehyde</b>					
Catalyst	Reaction conditions	%	Conversion	%	Selectivity
	Mole ratio/cat amt /temp/time	Glycerol		Dioxane	
1% MoO <sub>3</sub> /SiO <sub>2</sub> <sup>43</sup>	1.1:1/10 wt% /100 °C/480 min (solvent: toluene)	37		63	
10% MoO <sub>3</sub> /SiO <sub>2</sub> <sup>43</sup>	1.1:1/10 wt % /100 °C/480 min (solvent: toluene)	43		62.5	
20 % MoO <sub>3</sub> /SiO <sub>2</sub> <sup>43</sup>	1.1:1/10 wt% /100 °C/480 min (solvent: toluene)	72		60	
10% MoO <sub>3</sub> /TiO <sub>2</sub> - ZrO <sub>2</sub> <sup>44</sup>	1:1/5 wt % /100 °C/30 min	74		51	
TSA/nMCM-48 (Present work)	1:1/ 2.17 wt %/30 °C/40 min	95		65	
<b>Glycerol with furfural</b>					
SnO <sub>2</sub> <sup>45</sup>	1:1/5 wt %/20°C/30 min	51		38	
WO <sub>3</sub> /SnO <sub>2</sub> <sup>45</sup>	1:1/5 wt %/20°C/30 min	67		37	
MoO <sub>3</sub> /SnO <sub>2</sub> <sup>45</sup>	1:1/5 wt %/20°C/30 min	75		36	
TSA/nMCM-48 (Present work)	1:1/ 1.63 wt%/30°C/40 min	89		69	

### 3.9. Reaction mechanism

The probable reaction mechanism for acid catalysed acetalization of glycerol with benzaldehyde and furfural are shown in figure 13 For the reaction of glycerol with benzaldehyde, we have proposed the same mechanism as reported earlier by our group [23].

Similarly, for the acetalization of glycerol with furfural, the first step is initialized by the Bronsted acidity, proton present in TSA, which activates the carbonyl carbon of aldehyde. In the second step, the primary hydroxyl group of glycerol attacks the carbonyl carbon of aldehyde and forms hemiacetal. The subsequent formation of carbocation and removal of water molecule gives the dioxane derivative.

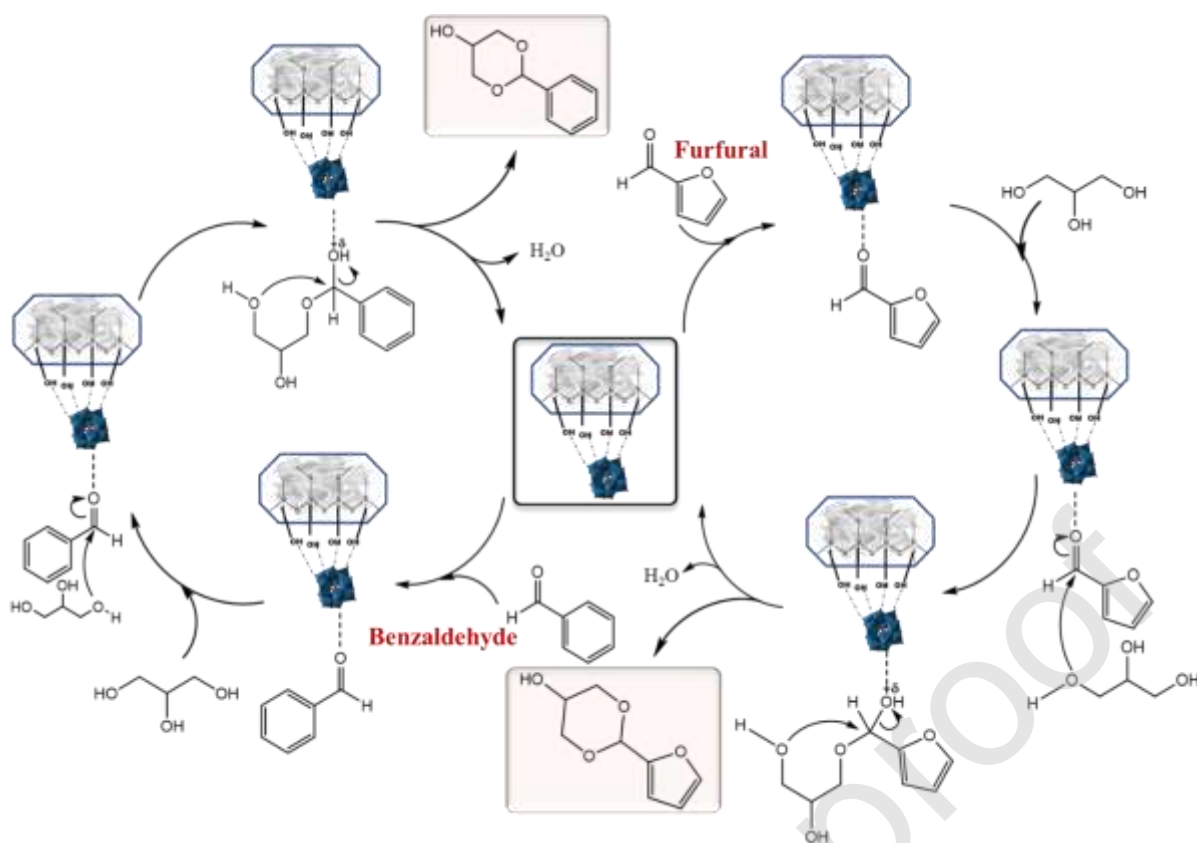


**Figure 13** Plausible reaction mechanism for acetalization of glycerol with benzaldehyde and furfural

#### 4. Conclusion

In a nutshell, first time nanoporous MCM-48 was successfully synthesized and used as a support for anchoring 12-tungstosilic acid. XRD, N<sub>2</sub>- sorption analysis and TEM confirms the 3D cubic geometry and nanoporosity of nMCM-48. Further, the interaction between TSA and nMCM-48 was established by BET as well as <sup>29</sup>Si MAS NMR. The synthesized catalyst was used for the synthesis of bio-fuel additives via catalytic valorisation of glycerol and the superiority of the catalyst lies in the inspiring results obtained at ambient reaction conditions. The obtained values of activation energy confirmed that both the reactions were truly governed by a chemical step. As compared to the reported ones, nMCM-48 proves to be better support due to its 3D geometry and nanoporosity which is responsible for higher selectivity of thermodynamically stable dioxane obtained for both the aldehydes. The catalyst was also recycled for consecutive four catalytic cycles and showed consistent conversion rate, thereby contributing effectively in the cost reduction of process as well as making the overall procedure sustainable and environmentally benign.

**Associated content**

The Supporting Information is available.

**Credit author statement**

**Anjali Patel:** Conceptualization, Reviewing and editing, Supervision

**Dhruvi Pithadia:** Methodology, Software, Writing-original draft preparation, Reviewing and editing.

**Conflict of Interest Disclosure**

There are no conflicts to declare.

**Acknowledgement**

We are thankful to Dr. N Lingaiah for NH<sub>3</sub>-TPD analysis at CSIR-IICT, Hyderabad. We are also thankful to Department of Chemistry, The Maharaja Sayajirao University of Baroda for BET surface area analysis and Sud-chemie India Pvt. Ltd., Nandesari, Vadodara for Powder XRD analysis.

**Declaration of interests**

The authors declare that they have no known competing financial interests or personal relationships that could have appeared to influence the work reported in this paper.

**References**

- [1] G. Morales, M. Paniagua, J.A. Melero, G. Vicente, C. Ochoa, *Ind. Eng. Chem. Res.* 50 (2011) 5898–5906.
- [2] B. Malleshham, P. Sudarsanam, B.M. Reddy, *Ind. Eng. Chem. Res.* 53 (2014) 18775–18785.
- [3] S.H. Chai, H.P. Wang, Y. Liang, B.Q. Xu, *J. Catal.* 250 (2007) 342–349.
- [4] I. Furikado, T. Miyazawa, S. Koso, A. Shimao, K. Kunimori, K. Tomishige, *Green Chem.* 9 (2007) 582–588.

- [5] S. Bagheri, N.M. Julkapli, W.A. Yehye, *Renew. Sustain. Energy Rev.* 41 (2015) 113–127.
- [6] Y. Wang, J. Zhou, X. Guo, *RSC Adv.* 5 (2015) 74611–74628.
- [7] U. Nda-Umar, I. Ramli, Y. Taufiq-Yap, E. Muhamad, *Catalysts* 9 (2018) 15.
- [8] M.R. Nanda, Z. Yuan, W. Qin, H.S. Ghaziaskar, M.A. Poirier, C.C. Xu, *Fuel* 117 (2014) 470–477.
- [9] A.R. Trifoi, P.Ş. Agachi, T. Pap, *Renew. Sustain. Energy Rev.* 62 (2016) 804–814.
- [10] A.J. Showler, P.A. Darley, *Chem. Rev.* 67 (1967) 427–440.
- [11] IEA (2019), *Tracking Transport*, IEA, Paris <https://www.iea.org/reports/tracking-transport-2019>
- [12] I.S. Gomes, D.C. de Carvalho, A.C. Oliveira, E. Rodríguez-Castellón, S. Tehuacanero-Cuapa, P.T.C. Freire, J.M. Filho, G.D. Saraiva, F.F. de Sousa, R. Lang, *Chem. Eng. J.* 334 (2018) 1927–1942.
- [13] V.T. Vasantha, N.J. Venkatesha, S.Z.M. Shamsuddin, J.Q. D’Souza, B.G.V. Reddy, *ChemistrySelect* 3 (2018) 602–608.
- [14] M.R. Nanda, Z. Yuan, W. Qin, H.S. Ghaziaskar, M.A. Poirier, C.C. Xu, *Appl. Energy* 123 (2014) 75–81.
- [15] M.S. Khayoon, B.H. Hameed, *Appl. Catal. A Gen.* 464–465 (2013) 191–199.
- [16] A. Talebian-Kiakalaieh, N.A.S. Amin, N. Najaafi, S. Tarighi, *Front. Chem.* 6 (2018) 1–25.
- [17] T.H. Abreu, C.I. Meyer, C. Padró, L. Martins, *Microporous Mesoporous Mater.* 273 (2019) 219–225.
- [18] K.S. Arias, A. Garcia-Ortiz, M.J. Climent, A. Corma, S. Iborra, *ACS Sustain. Chem. Eng.* 6 (2018) 4239–4245.
- [19] A. Talebian-Kiakalaieh, S. Tarighi, *J. Ind. Eng. Chem.* 79 (2019) 452–464.
- [20] J.E. Castanheiro, J. Vital, I.M. Fonseca, A.M. Ramos, *Catal. Today* (2019) <https://doi.org/10.1016/j.cattod.2019.04.048>.
- [21] L. Chen, B. Nohair, D. Zhao, S. Kaliaguine, *ChemCatChem* 10 (2018) 1918–1925.
- [22] L. Chen, B. Nohair, D. Zhao, S. Kaliaguine, *Appl. Catal. A Gen.* 549 (2018) 207–215.
- [23] N. Narkhede, A. Patel, *Appl. Catal. A Gen.* 515 (2016) 154–163.

- [24] L. Chen, B. Nohair, S. Kaliaguine, *Appl. Catal. A Gen.* 509 (2016) 143–152.
- [25] F. Zhang, Y. Jin, J. Shi, Y. Zhong, W. Zhu, M.S. El-Shall, *Chem. Eng. J.* 269 (2015) 236–244.
- [26] M.J. da Silva, A.A. Julio, F.C.S. Dorigetto, *RSC Adv.* 5 (2015) 44499–44506.
- [27] N. Narkhede, A. Patel, *RSC Adv.* 4 (2014) 19294–19301.
- [28] P. Ferreira, I.M. Fonseca, A.M. Ramos, J. Vital, J.E. Castanheiro, *Appl. Catal. B Environ.* 98 (2010) 94–99.
- [29] E. Gutiérrez-Acebo, F. Guerrero-Ruiz, M. Centenero, J.S. Martínez, P. Salagre, Y. Cesteros, *Open Chem.* 16 (2018) 386–392.
- [30] D. Kumar, K. Schumacher, C. Du Fresne von Hohenesche, M. Grün, K.K. Unger, *Colloids Surfaces A Physicochem. Eng. Asp.* 187–188 (2001) 109–116.
- [31] N. You, J.H. Yim, S.J. Lee, J.H. Lee, Y.K. Park, J.K. Jeon, in: *J. Nanosci. Nanotechnol.*, 2007, pp. 3800–3804.
- [32] S. Singh, A. Patel, *J. Clean. Prod.* 72 (2014) 46–56.
- [33] Y. Zhang, S. Yang, *J. Wuhan Univ. Technol. Mater. Sci. Ed.* 23 (2008) 346–349.
- [34] D. Bajuk-Bogdanović, I. Holclajtner-Antunović, M. Todorović, U.B. Mioč, J. Zakrzewska, *J. Serbian Chem. Soc.* 73 (2008) 197–209.
- [35] M. Thommes, K. Kaneko, A. V. Neimark, J.P. Olivier, F. Rodriguez-Reinoso, J. Rouquerol, K.S.W. Sing, *Pure Appl. Chem.* 87 (2015) 1051–1069.
- [36] V. Zeleňák, D. Halamová, M. Almáši, L. Žid, A. Zeleňáková, O. Kapusta, *Appl. Surf. Sci.* 443 (2018) 525–534.
- [37] J. Xu, Z. Luan, H. He, W. Zhou, L. Kevan, *Chem. Mater.* 10 (1998) 3690–3698.
- [38] A. Sakthivel, K. Komura, Y. Sugi, *Ind. Eng. Chem. Res.* 47 (2008) 2538–2544.
- [39] D. Carriazo, C. Domingo, C. Martín, V. Rives, *J. Solid State Chem.* 181 (2008) 2046–2057.
- [40] V. Dellarocca, L. Marchese, M.L. Peña, F. Rey, A. Corma, S. Coluccia, *Stud. Surf. Sci. Catal.* 140 (2001) 209–220.
- [41] F.J. Berry, G.R. Derrick, M. Mortimer, *Polyhedron* 68 (2014) 17–22.
- [42] G.C. Bond, *Heterogeneous catalysis: principles and applications*, Clarendon Press, Oxford, 1974.

- [43] S.B. Umbarkar, T. V. Kotbagi, A. V. Biradar, R. Pasricha, J. Chanale, M.K. Dongare, A.S. Mamede, C. Lancelot, E. Payen, *J. Mol. Catal. A Chem.* 310 (2009) 150–158.
- [44] P. Sudarsanam, B. Mallesham, A.N. Prasad, P.S. Reddy, B.M. Reddy, *Fuel Process. Technol.* 106 (2013) 539–545.
- [45] B. Mallesham, P. Sudarsanam, G. Raju, B.M. Reddy, *Green Chem.* 15 (2013) 478–489.

Journal Pre-proof